Prior-Guided Residual Diffusion: Calibrated and Efficient Medical Image Segmentation

Fuyou Mao*, Beining Wu†[1], Yanfeng Jiang‡, Han Xue†, Yan Tang*, and Hao Zhang*
*School of Electronic Information, Central South University, Changsha, China
†Hangzhou Dianzi University, Hangzhou, China
‡Communication University of Zhejiang, China
Email: maoeyu@csu.edu.cn, 24320125@hdu.edu.cn

***Abstract*—Ambiguity in medical image segmentation calls for models that capture full conditional distributions rather than a single point estimate. We present *Prior-Guided Residual Diffusion* (PGRD), a diffusion-based framework that learns voxel-wise distributions while maintaining strong calibration and practical sampling efficiency. PGRD embeds discrete labels as one-hot targets in a continuous space to align segmentation with diffusion modeling. A coarse prior predictor provides step-wise guidance; the diffusion network then learns the residual to the prior, accelerating convergence and improving calibration. A deep diffusion supervision scheme further stabilizes training by supervising intermediate time steps. Evaluated on representative MRI and CT datasets, PGRD achieves higher Dice scores and lower NLL/ECE values than Bayesian, ensemble, Probabilistic U-Net, and vanilla diffusion baselines, while requiring fewer sampling steps to reach strong performance.**

***Index Terms*—Medical image segmentation, diffusion models, uncertainty estimation, calibration, sampling efficiency**

I. Introduction

In modern clinical practice, medical image segmentation is an indispensable technology for critical procedures such as diagnosis, treatment planning, and disease monitoring [1], [2]. However, the segmentation task often faces significant uncertainty due to inherent noise and artifacts in medical images, as well as the inter-observer variability among clinical experts manually delineating anatomical structures or lesions. Traditional deterministic segmentation models typically output a single, most probable class label for each pixel or voxel, forming a single segmentation map [3], [4]. While intuitive, this approach has a fundamental flaw: it cannot express or quantify the uncertainty in its predictions. Furthermore, its predictions are often over-confident, which can introduce potential risks in safety-critical clinical decision-making. Therefore, it is of paramount importance to develop probabilistic segmentation models capable of capturing and modeling this uncertainty—that is, learning a conditional distribution over all plausible segmentation given an input image.

To achieve probabilistic modeling, the academic community has explored various technical paths [5]. Mainstream methods can be broadly categorized into three types: (i) Bayesian Neural Networks [6], which approximate the posterior distribution by sampling model parameters; (ii) Deep Ensembles [7] and Multi-Head Models [8], which construct a structured hypothesis space by training multiple independent models or setting up multiple outputs within a single model; and (iii) generative models such as Generative Adversarial Networks (GANs) or Conditional Variational Autoencoders (CVAEs) [9]. Although these methods have, to some extent, enhanced the model's ability to express uncertainty, they each have inherent limitations. For instance, Bayesian methods are computationally expensive and rely on the quality of approximate inference; Deep Ensembles consume substantial training and inference resources; and GAN/VAE-based generative models often suffer from training instability, mode collapse, or poor probability calibration. Consequently, there is an urgent need in the field for a novel solution that can balance the diversity of generated results, training stability, and probability calibration.

Denoising Diffusion Probabilistic Models (DDPMs) [10], or simply diffusion models, have garnered significant attention as a powerful class of generative models due to their outstanding performance and stable training process in high-dimensional data generation tasks, especially with natural images [11]. However, directly applying standard diffusion models to medical image segmentation presents two core challenges [12], [13]: First, output space mismatch. Diffusion models naturally operate in a continuous data space, whereas image segmentation is fundamentally a pixel-wise or voxel-wise discrete classification problem. Effectively bridging the continuous diffusion process with discrete segmentation labels is a key challenge. Second, low computational efficiency. The generation process of diffusion models relies on an iterative reverse denoising chain, often requiring hundreds or even thousands of steps to produce high-quality samples. For time-sensitive clinical applications, the associated computational cost can be prohibitively high.

To address these challenges, this paper proposes a novel diffusion model framework tailored for medical image segmentation that emphasizes both probability calibration and sampling efficiency—the Prior-Guided Residual Diffusion (PGRD) model. Our core idea is to decompose the complex task of segmentation map generation. First, we resolve the output space mismatch by embedding discrete segmentation labels as one-hot vectors, cleverly transforming them into diffusion targets that can be processed in a continuous space. Second, and

These authors contributed equally to this work.
Hao Zhang is the corresponding author.

our main innovation, we introduce a lightweight prior network that provides a coarse segmentation prediction at each step of the diffusion process. Consequently, the powerful diffusion model no longer needs to learn the entire complex segmentation map from pure noise but instead focuses on learning the residual between the ground truth and the coarse prior. This residual learning paradigm greatly simplifies the model's learning objective, thereby significantly reducing the number of sampling steps required for convergence and improving the calibration of the final predictions. Furthermore, we have designed a Deep Diffusion Supervision (DDS) mechanism, which applies additional supervisory signals at intermediate steps of the denoising process to further stabilize model optimization and guide the model to more accurately recover the clean segmentation label throughout the entire chain [14].

The experiments in this paper will be conducted on several public Magnetic Resonance Imaging (MRI) and Computed Tomography (CT) datasets. The results will demonstrate that, compared to various Bayesian methods, deep ensembles, Probabilistic U-Net, and standard diffusion model baselines, PGRD not only achieves superior performance in segmentation accuracy (e.g., Dice Similarity Coefficient) but also shows better performance on key probability calibration metrics (such as Negative Log-Likelihood, NLL, and Expected Calibration Error, ECE). Moreover, all of this is achieved while requiring fewer sampling steps. Our contributions can be seen as follows:

- **Segmentation-aware diffusion targets.** We embed labels as one-hot vectors in a continuous space, enabling diffusion to learn voxel-wise distributions while remaining compatible with discrete evaluation.
- **Prior-guided residual learning (PGR).** A light prior network provides coarse segmentations at each step; the diffusion model learns only the residual to the prior, reducing required sampling steps and improving calibration.
- **Deep diffusion supervision (DDS).** We supervise intermediate time steps to stabilize optimization and encourage accurate recovery of the clean label along the chain.

II. Method

A. Overview and Problem Setup

Let x denote an input 2D/3D image volume and y the corresponding discrete segmentation. We represent y as a one-hot vector field y_0 (per voxel), which serves as the diffusion target in a continuous space. A prior predictor $g_\varphi(x)$ provides step-wise guidance; the diffusion model parameterized by θ learns to recover y_0 from noisy states while leveraging the prior.

B. RGRM: Prior-Guided Residual Diffusion Model

We call the per-step Residual Guided RefineMent the RGRM module. It operates on the residual state $\mathbf{r}_t := \mathbf{s}_t - \pi_\phi(\mathbf{X})$. Forward (noising) with prior drift. At every step the forward transition is biased toward the prior

$$q(\mathbf{s}_t \mid \mathbf{s}_{t-1}, \mathbf{X}) = \mathcal{N}\big(\rho_t\, \mathbf{s}_{t-1} + (1-\rho_t)\, \pi_\phi(\mathbf{X}),\ \sigma_t^2 \mathbf{I}\big). \quad (1)$$

This induces a residual marginal that stays near the prior manifold:

$$\mathbf{r}_t = \sqrt{\bar\rho_t}\, \mathbf{r}_0 + \sqrt{1-\bar\rho_t}\, \boldsymbol{\varepsilon}, \qquad \boldsymbol{\varepsilon} \sim \mathcal{N}(\mathbf{0}, \mathbf{I}), \quad (2)$$

so learning reduces to the clean residual $\mathbf{r}_0 = \mathbf{y}_\star - \pi_\phi(\mathbf{X})$.

a) Noise parameterization around the prior.: Instead of predicting noise or $\mathbf{y}_\star$, RGRM predicts a *noise* on the residual channel:

$$\mathbf{v}_t := \sqrt{\bar\rho_t}\, \boldsymbol{\varepsilon} - \sqrt{1-\bar\rho_t}\, \mathbf{r}_0. \quad (3)$$

From $(\mathbf{r}_t, \mathbf{v}_t)$ we recover

$$\mathbf{r}_0 = \sqrt{\bar\rho_t}\, \mathbf{r}_t - \sqrt{1-\bar\rho_t}\, \mathbf{v}_t, \quad \boldsymbol{\varepsilon} = \sqrt{1-\bar\rho_t}\, \mathbf{r}_t + \sqrt{\bar\rho_t}\, \mathbf{v}_t. \quad (4)$$

The RGRM network f_θ outputs $\widehat{\mathbf{v}}_t = f_\theta(\mathbf{s}_t, \mathbf{X}, \pi_\phi(\mathbf{X}), t)$; we then obtain $\widehat{\mathbf{r}}_0$ via (4) and the clean estimate $\widehat{\mathbf{y}}_0 = \pi_\phi(\mathbf{X}) + \widehat{\mathbf{r}}_0$.

b) Reverse (denoising) step.: Using the DDPM posterior with our centered variables:

$$\boldsymbol{\mu}_\theta(\mathbf{s}_t, \widehat{\mathbf{y}}_0, t) = \frac{\sqrt{\bar\rho_{t-1}}\,(1-\rho_t)}{1-\bar\rho_t}\, \widehat{\mathbf{y}}_0 + \frac{\sqrt{\rho_t}\,(1-\bar\rho_{t-1})}{1-\bar\rho_t}\, \mathbf{s}_t, \quad (5)$$
$$\sigma_t^2 \in \{1-\rho_t,\ \tilde\sigma_t^2\}.$$

We sample $\mathbf{s}_{t-1} = \boldsymbol{\mu}_\theta + \sigma_t \mathbf{z}$ with $\mathbf{z} \sim \mathcal{N}(0, \mathbf{I})$; a DDIM-style sampler sets $\sigma_t = 0$.

C. Deep Diffusion Supervision (DDS)

At steps $t \in \mathcal{T}$, an auxiliary head ψ_t outputs logits; with temperature τ, $\hat{\mathbf{y}}_0^{(t)} = \mathrm{softmax}(\psi_t/\tau)$. The DDS loss is

$$\mathcal{L}_{\mathrm{DDS}} = \sum_{t \in \mathcal{T}} \mathrm{CE}\big(\hat{\mathbf{y}}_0^{(t)},\ \mathbf{y}_\star\big). \quad (6)$$

D. Training Objective

We use a *noise* loss plus DDS. First construct

$$\mathbf{s}_t = \sqrt{\bar\rho_t}\, \mathbf{y}_\star + \big(1 - \sqrt{\bar\rho_t}\big)\pi_\phi(\mathbf{X}) + \sigma_t\, \boldsymbol{\varepsilon}, \quad (7)$$

then minimize

$$\mathcal{L}_{\mathrm{vel}} = \mathbb{E}_{t, \mathbf{y}_\star, \boldsymbol{\varepsilon}} \big\| \mathbf{v}_t - f_\theta(\mathbf{s}_t, \mathbf{X}, \pi_\phi(\mathbf{X}), t) \big\|_2^2, \quad (8)$$

and combine with DDS:

$$\mathcal{L}_{\mathrm{total}} = \mathcal{L}_{\mathrm{vel}} + \lambda\, \mathcal{L}_{\mathrm{DDS}}, \qquad \lambda > 0. \quad (9)$$

E. Inference and Aggregation

At test time we inject the prior at *every* reverse step and draw M samples by iterating $\mathbf{s}_{t-1} = \boldsymbol{\mu}_\theta(\mathbf{s}_t, \widehat{\mathbf{y}}_0, t) + \sigma_t \mathbf{z}$. The final mask is obtained from the voxel-wise mean probability $\bar{\mathbf{p}} = \frac{1}{M} \sum_m \mathrm{softmax}(\hat{\mathbf{y}}_0^{(m)}/\tau_{\mathrm{out}})$ followed by $\arg\max$.

We modify the forward noising process to inject the prior at each time step so that states remain near a coarse segmentation manifold. Rather than denoise from pure noise, the model denoises from a mixture of the previous state and the prior prediction, making the reverse process focus on learning the residual to the prior, which accelerates sampling and improves calibration. In practice, this is realized by adjusting the mean of the forward transition to a convex combination of the previous state and $g_\varphi(x)$, with variance schedule $\{\beta_t\}$:

$$q(\mathbf{y}_t \mid \mathbf{y}_{t-1}, g_\varphi(x)) = \mathcal{N}\big(\alpha_t\, \mathbf{y}_{t-1} + (1-\alpha_t)\, g_\varphi(x),\ \beta_t \mathbf{I}\big). \quad (10)$$

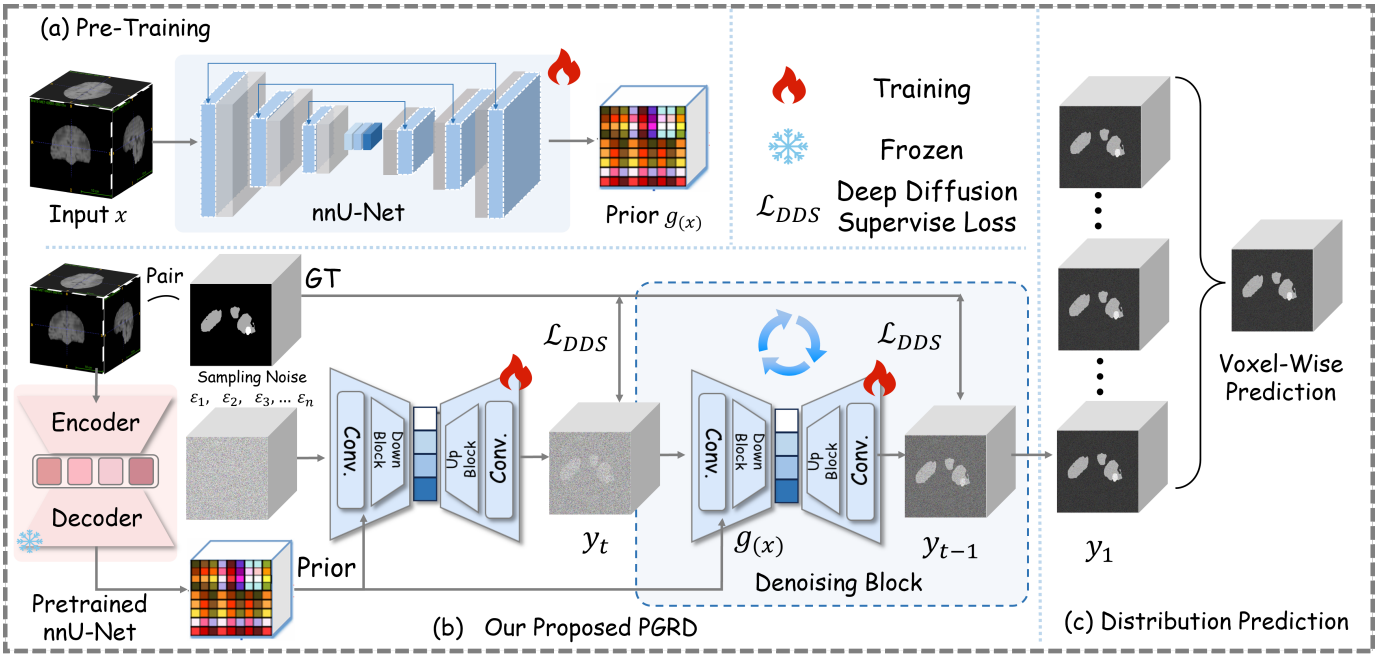

Fig. 1. **Illustration of the Prior-Guided Residual Diffusion (PGRD) pipeline for probabilistic medical image segmentation.** Our method decomposes the complex segmentation task into a two-step process. First, as shown in panel (a), a deterministic nnU-Net is pre-trained to provide a reliable but coarse prior $g(x)$. Then, in panel (b), this prior guides the reverse diffusion process. Instead of learning the entire segmentation from noise, our denoising U-Net focuses on the simpler task of learning the residual between the current noisy state y_t and the prior. This residual learning is further stabilized by our Deep Diffusion Supervision (DDS) mechanism. As depicted in panel (c), repeating this guided denoising process allows us to sample multiple plausible segmentation maps, effectively capturing the underlying uncertainty in the data and yielding a well-calibrated predictive distribution.

TABLE I
SEGMENTATION AND CALIBRATION ON BRATS2024 AND INSTANCE2022 (MEAN±STD). LOWER IS BETTER FOR NLL/ECE. BEST RESULTS IN **BOLD**.

Methods	BraTS2024			INSTANCE2022		
	DSC(%)	NLL(%)	ECE(%)	DSC(%)	NLL(%)	ECE(%)
Baseline	75.8±22.4	4.9±1.3	0.24±0.13	53.7±12.5	2.00±0.54	0.86±0.12
MC Dropout [15]	76.9±27.2	4.4±1.5	0.22±0.14	54.1±21.2	1.40±0.43	0.88±0.31
Deep Ens [16]	80.0±21.5	4.9±1.0	0.21±0.16	58.7±17.8	1.10±0.47	0.84±0.22
M-Heads [17]	78.0±18.6	4.7±2.4	0.21±0.13	57.6±19.6	1.50±0.32	0.93±0.26
Prob. U-Net [18]	79.3±19.8	5.1±3.1	0.20±0.17	59.2±20.4	1.20±0.45	0.72±0.18
DDPM [19]	78.3±24.3	4.8±1.8	0.23±0.13	59.8±19.3	1.12±0.32	0.68±0.26
PGRD w/o PGR	79.2±24.6	4.8±1.6	0.22±0.14	60.2±17.8	1.22±0.25	0.73±0.21
PGRD w/o DDS	80.6±36.5	4.4±1.7	0.21±0.16	61.5±23.4	1.13±0.35	0.69±0.17
Ours (PGRD)	81.7±26.8	4.2±1.3	0.20±0.12	62.2±21.8	1.00±0.23	0.65±0.24

The reverse process is parameterized as

$$p_\theta(\mathbf{y}_{t-1} \mid \mathbf{y}_t, x, g_\varphi(x)) = \mathcal{N}\big(\mu_\theta(\mathbf{y}_t, x, g_\varphi(x), t),\, \Sigma_\theta(t)\big). \tag{11}$$

Intuitively, μ_θ learns the residual to the prior, i.e., $\mu_\theta \approx \mathbf{y}_t - \epsilon_\theta(\mathbf{y}_t, x, t) + \lambda_t(g_\varphi(x) - \mathbf{y}_t)$.

F. Deep Diffusion Supervision (DDS)

To encourage faithful recovery of y_0 throughout the chain, we attach light decoder heads at selected time steps and apply cross-entropy supervision after a softmax on the reconstructed $\hat{y}_0$. This intermediate supervision improves gradients early in training and reduces exposure bias.

III. EXPERIMENTS

A. Datasets and Metrics

Datasets. This study utilizes two publicly available medical imaging datasets. Specifically, we use the BraTS 2024 dataset [20], which comprises 351 cases of multi-modal brain MRI scans, and the INSTANCE 2022 [21] benchmark, which contains 200 cases of non-contrast head CT scans. Evaluation Metrics. To comprehensively evaluate the model's distribution learning performance, we adopt three standard metrics: the Dice Similarity Coefficient (DSC) to measure segmentation accuracy, and the Negative Log Likelihood (NLL) and Expected Calibration Error (ECE) to assess the reliability of the predicted

probabilities.

B. Implementation Details

Models are implemented in PyTorch and trained on NVIDIA GeForce RTX 4090 GPUs using Adam. We adopt a 3D U-Net-like prior/baseline for MRI [22] and a 2D U-Net variant for CT [23]. The prior is trained first to convergence and then frozen while training PGRD. Unless otherwise noted, learning rate 1×10^{-3}, batch size 2, and supervision weight $\lambda = 0.1$.Our training procedure employs a two-stage strategy. In the first stage, we independently train the diffusion prior prediction model until convergence. In the second stage, we freeze the weights of this prior model and integrate it into the complete PGRD framework for end-to-end training. We adopt a T=1000-step forward process with the cosine noise schedule [24]: $\beta_t \in (0, 1)$, $\alpha_t = 1 - \beta_t$, and $\bar{\alpha}_t = \prod_{k=1}^{t} \alpha_k$. Our method uses the v-parameterization; the network predicts $v_\theta(x_t, t)$ and we recover $\hat{x}_0$ in the standard way. Unless otherwise specified, we sample with S=300 denoising steps on a uniformly spaced subset $\mathcal{T} = \{t_1 < \cdots < t_S\} \subset \{1, \ldots, T\}$ using DDIM (η=0). Baselines that require DDPM sampling use the full T=1000 steps. We used a consistent learning rate of 0.001 and a batch size of 2 for both datasets. For data pre-processing, we adopted the methods described in [22] and [23] for BraTS2024 and INSTANCE2022, respectively. To address the scale disparity between different loss functions, we introduced a weighting factor λ, which was set to 0.1 as it empirically yielded the best model performance.

C. Baselines and Ablations

Baselines. Deterministic U-Net variants; MC Dropout; Deep Ensemble; Multi-Head models; Probabilistic U-Net; and vanilla DDPM adapted to segmentation.
Ablations. (i) *w/o PGR* (remove prior injection); (ii) *w/o DDS* (remove intermediate supervision).

D. Evaluation Protocols

We report mean±std across cases. For statistical testing we use paired t-tests vs. competitive baselines. For sampling efficiency, we plot Dice vs. number of sampling steps. Calibration is analyzed via NLL/ECE and error–uncertainty correlations.

IV. Results

A. Overall Performance

PGRD improves Dice while reducing NLL and ECE across datasets relative to Bayesian, ensemble, multi-head, Probabilistic U-Net, and vanilla DDPM baselines. Gains are consistent across structures and statistically significant on key metrics.

As shown in Table I, our proposed PGRD model demonstrates superior performance across both the BraTS2024 and INSTANCE2022 datasets. On BraTS2024, PGRD achieves the highest Dice Similarity Coefficient (DSC) of 81.7%, surpassing the strongest baseline (Deep Ensembles at 80.0%) by 1.7%. More importantly, our method obtains the best calibration scores, with the lowest Negative Log-Likelihood (NLL) of 4.2% and the lowest Expected Calibration Error (ECE) of 0.20%. A similar trend is observed on the INSTANCE2022 dataset, where PGRD not only leads in segmentation accuracy with a DSC of 62.2% but also achieves state-of-the-art calibration performance (NLL: 1.00%, ECE: 0.65%). These results empirically validate that our prior-guided residual learning framework can significantly enhance both segmentation accuracy and the reliability of uncertainty estimation compared to existing probabilistic and diffusion-based models.

B. Ablation Studies

To validate the effectiveness of our key contributions, we conducted ablation studies on the two main components of PGRD: Prior-Guided Residual Diffusion (PGRD w/o PGR) and Deep Diffusion Supervision (PGRD w/o DDS). The results in Table I reveal that removing the prior guidance (PGRD w/o PGR) leads to a noticeable drop in performance on both datasets. For instance, on INSTANCE2022, DSC decreases from 62.2% to 60.2%, and NLL increases from 1.00% to 1.22%, indicating that the prior-guided mechanism is crucial for improving both accuracy and calibration. Similarly, removing the deep supervision (PGRD w/o DDS) also results in performance degradation (e.g., BraTS2024 DSC drops from 81.7% to 80.6%), confirming that intermediate supervision effectively stabilizes the training process and guides the model toward a better optimum. The comprehensive performance of the full PGRD model underscores the synergistic effect of these two components.

C. Sampling Efficiency and Qualitative Analysis

Figure 3 highlights our model's superior sampling efficiency. PGRD consistently reaches high DSC scores with substantially fewer denoising steps compared to baselines. For instance, it achieves near-peak performance at around 300 steps, while the vanilla DDPM requires over 800 steps. This efficiency is primarily attributed to our PGR mechanism, as the model without it (PGRD w/o PGR) performs similarly to the slow-converging DDPM. This rapid convergence demonstrates a clear computational advantage for practical deployment.

V. Conclusion

We have presented PGRD a new diffusion-based approach that successfully addresses the critical challenges of calibration and efficiency in probabilistic medical image segmentation. Our key innovation lies in the prior-guided residual learning paradigm, which simplifies the modeling task by having the diffusion network learn corrections to a coarse, pre-computed prior. This design choice, combined with a segmentation-aware one-hot embedding and a stabilizing deep supervision loss, leads to a model that not only generates highly accurate and well-calibrated segmentation distributions but does so with remarkable sampling efficiency. As empirically validated on diverse medical datasets, PGRD sets a new state-of-the-art, demonstrating that properly structured guidance can unlock the potential of diffusion models for safety-critical clinical applications where both accuracy and trustworthy uncertainty are paramount.

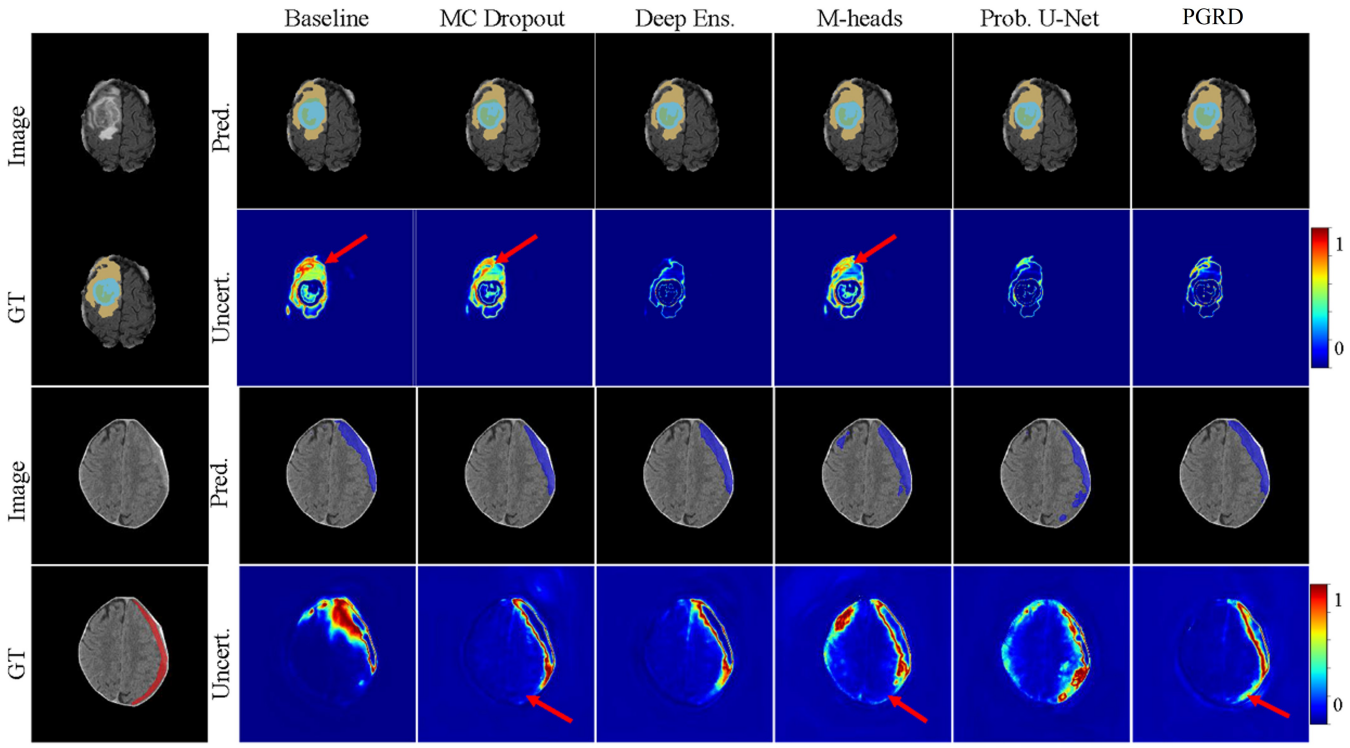

Fig. 2. Qualitative comparison of segmentation and uncertainty maps on two representative cases from the BraTS2024 (top) and INSTANCE2022 (bottom).

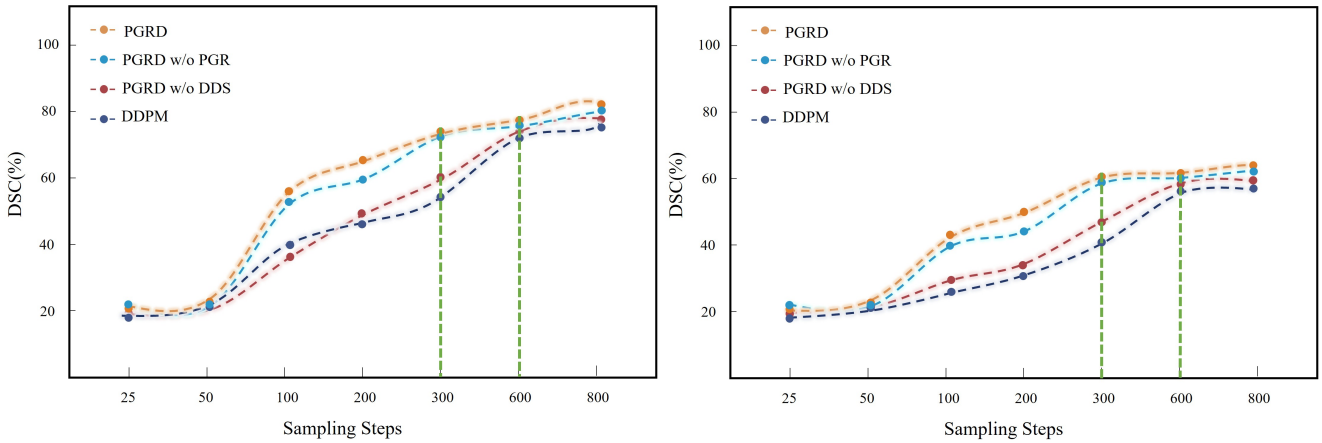

Fig. 3. DSC versus the number of sampling steps demonstrates the superiority of efficiency for PGRD. BraTS2024(left) and INSTANCE2022(right)

ACKNOWLEDGMENT

REFERENCES

[1] Q. Xia, H. Zheng, H. Zou, D. Luo, H. Tang, L. Li, and B. Jiang, "A comprehensive review of deep learning for medical image segmentation," *Neurocomputing*, vol. 613, p. 128740, 2025.

[2] S. Kumar, "Advancements in medical image segmentation: A review of transformer models," *Computers and Electrical Engineering*, vol. 123, p. 110099, 2025.

[3] X.-H. Le, D. Van Binh, and G. Lee, "Performance and uncertainty analysis in deep learning frameworks for streamflow forecasting via monte carlo dropout technique," *Journal of Hydrology: Regional Studies*, vol. 61, p. 102668, 2025.

[4] F. Mao, L. Lin, M. Jiang, D. Dai, C. Yang, H. Zhang, and Y. Tang, "Cross-modal medical image generation based on pyramid convolutional attention network," 2024. [Online]. Available: https://arxiv.org/abs/2411.17420

[5] D. Tran, A. Kucukelbir, A. B. Dieng, M. Rudolph, D. Liang, and D. M. Blei, "Edward: A library for probabilistic modeling, inference, and criticism," *arXiv preprint arXiv:1610.09787*, 2016.

[6] Y. Kwon, J.-H. Won, B. J. Kim, and M. C. Paik, "Uncertainty quantification using bayesian neural networks in classification: Application to biomedical image segmentation," *Computational Statistics & Data Analysis*, vol. 142, p. 106816, 2020.

[7] L. Nanni, D. Cuza, A. Lumini, A. Loreggia, and S. Brahnam, "Deep ensembles in bioimage segmentation," *arXiv preprint arXiv:2112.12955*, 2021.

[8] S. Masaki, T. Hirakawa, T. Yamashita, and H. Fujiyoshi, "Multi-domain semantic-segmentation using multi-head model," in *2021 IEEE international intelligent transportation systems conference (ITSC)*. IEEE, 2021, pp. 2802–2807.

[9] A. A. Pol, V. Berger, C. Germain, G. Cerminara, and M. Pierini, "Anomaly detection with conditional variational autoencoders," in *2019 18th IEEE international conference on machine learning and applications (ICMLA)*. IEEE, 2019, pp. 1651–1657.

[10] Y. Li, Z. Yu, G. He, Y. Shen, K. Li, X. Sun, and S. Lin, "Spd-ddpm: Denoising diffusion probabilistic models in the symmetric positive definite space," in *Proceedings of the AAAI conference on artificial intelligence*, vol. 38, no. 12, 2024, pp. 13 709–13 717.

[11] L. Zhang, F. Wu, K. Bronik, and B. W. Papiez, "Diffuseg: domain-driven diffusion for medical image segmentation," *IEEE Journal of Biomedical and Health Informatics*, 2025.

[12] C. Wang, X. Li, H. Ding, L. Qi, J. Zhang, Y. Tong, C. C. Loy, and S. Yan, "Explore in-context segmentation via latent diffusion models," in *Proceedings of the AAAI Conference on Artificial Intelligence*, vol. 39, no. 7, 2025, pp. 7545–7553.

[13] Y. Mao, J. Zhang, M. Xiang, Y. Lv, D. Li, Y. Zhong, and Y. Dai, "Contrastive conditional latent diffusion for audio-visual segmentation," *IEEE Transactions on Image Processing*, 2025.

[14] S. Ren, F. Wei, S. A. Z. Zhang, and H. Hu, "Deepmim: Deep supervision for masked image modeling," in *2025 IEEE/CVF Winter Conference on Applications of Computer Vision (WACV)*. IEEE, 2025, pp. 879–888.

[15] Y. Gal and Z. Ghahramani, "Dropout as a bayesian approximation: Representing model uncertainty in deep learning," 2016. [Online]. Available: https://arxiv.org/abs/1506.02142

[16] B. Lakshminarayanan, A. Pritzel, and C. Blundell, "Simple and scalable predictive uncertainty estimation using deep ensembles," *Advances in neural information processing systems*, vol. 30, 2017.

[17] C. Rupprecht, I. Laina, R. DiPietro, M. Baust, F. Tombari, N. Navab, and G. D. Hager, "Learning in an uncertain world: Representing ambiguity through multiple hypotheses," in *Proceedings of the IEEE international conference on computer vision*, 2017, pp. 3591–3600.

[18] S. Kohl, B. Romera-Paredes, C. Meyer, J. De Fauw, J. R. Ledsam, K. Maier-Hein, S. Eslami, D. Jimenez Rezende, and O. Ronneberger, "A probabilistic u-net for segmentation of ambiguous images," *Advances in neural information processing systems*, vol. 31, 2018.

[19] J. Ho, A. Jain, and P. Abbeel, "Denoising diffusion probabilistic models," *Advances in neural information processing systems*, vol. 33, pp. 6840–6851, 2020.

[20] B. Bonato, L. Nanni, and A. Bertoldo, "Advancing precision: A comprehensive review of mri segmentation datasets from brats challenges (2012–2025)," *Sensors (Basel, Switzerland)*, vol. 25, no. 6, p. 1838, 2025.

[21] N. Guo, Y. Liu, P. Zhang, J. Kang, Z. Gui, and L. Wang, "3d medical image segmentation based on group mixing dual attention," *Biomedical Signal Processing and Control*, vol. 110, p. 107985, 2025.

[22] F. Isensee, P. Kickingereder, W. Wick, M. Bendszus, and K. H. Maier-Hein, "No new-net," in *International MICCAI brainlesion workshop*. Springer, 2018, pp. 234–244.

[23] X. Li, G. Luo, W. Wang, K. Wang, Y. Gao, and S. Li, "Hematoma expansion context guided intracranial hemorrhage segmentation and uncertainty estimation," *IEEE Journal of Biomedical and Health Informatics*, vol. 26, no. 3, pp. 1140–1151, 2021.

[24] S. Lin, B. Liu, J. Li, and X. Yang, "Common diffusion noise schedules and sample steps are flawed," in *Proceedings of the IEEE/CVF winter conference on applications of computer vision*, 2024, pp. 5404–5411.